Impact of penetrative solar radiation on the diagnosis of water mass transformation in the Mediterranean Sea

Alexandra Bozec, Pascale Bouruet-Aubertot, Daniele Iudicone, Michel Crépon

Impact of penetrative solar radiation on the diagnosis of water mass transformation in the Mediterranean Sea

Alexandra Bozec,[1,3] Pascale Bouruet-Aubertot,[1] Daniele Iudicone,[2] and Michel Crépon[1]

Received 23 October 2007; revised 24 January 2008; accepted 13 February 2008; published 13 June 2008.

[1] We applied a revised diagnosis of water mass formation and mixing to a 1/8° resolution ocean model of the Mediterranean Sea. The diagnosis method used and presented by Iudicone et al. (2008) is similar to that developed by Walin (1982) and applied to the Mediterranean Sea by Tziperman and Speer (1994), to which we added a penetrative solar radiation. Both the prognostic model and the diagnostic method were in agreement with respect to the solar flux parameterization. Major changes were observed in the yearly budget of water mass transformation when the penetrative solar radiation is taken into account in the diagnosis. Annual estimates of water mass formation rates were decreased by a factor of two, with values within the range [−3.7 Sv, 1.5 Sv] compared to [−6 Sv, 3 Sv]. This decrease resulted from a lower seasonal variation when penetrative solar radiation was included. This can be explained by the fact that the solar radiation flux acted over a wider range of seawater density leading to lower net values over a given density interval. The major impact of the penetrative solar radiation occurred during spring and summer. Newly formed dense water was then transformed into lighter water with a rate reaching a value about 50% of that of the water mass formation rate in winter. Another consequence was that mixing processes which counteract formation rate in yearly budget of water mass formation rates, were overestimated. We showed that, in spring and summer, about a third of the transformation took place below the surface layer.

Citation: Bozec, A., P. Bouruet-Aubertot, D. Iudicone, and M. Crépon (2008), Impact of penetrative solar radiation on the diagnosis of water mass transformation in the Mediterranean Sea, *J. Geophys. Res.*, *113*, C06012, doi:10.1029/2007JC004606.

1. Introduction

[2] Solar radiation is one of the main forcing factors that drive the ocean circulation, through the creation of horizontal density gradients and water mass formation. How this solar radiation is absorbed in the first hundred meters of the ocean basically depends on the pigments and particle concentration of the seawater [*Jerlov*, 1968; *Morel and Antoine*, 1994; *Frouin and Iacobellis*, 2002]. This penetrative radiation is of particular importance in regions with a shallow mixed layer, such as tropical regions, as evidenced by *Lewis et al.* [1990] and later by *Murtugudde et al.* [2002]. In particular, *Lewis et al.* [1990] showed that the introduction of a penetrative solar radiation into models greatly improved the estimate of the sea-surface temperature in the tropical Pacific Ocean. This results from the fact that a nonnegligible amount of the net heat flux is absorbed below the surface leading to a decrease in the sea surface temperature with respect to the non penetrative solar case. Also, this redistribution of heat into deep water could be of primary importance in water mass transformation [*Iudicone et al.*, 2008]. For instance an overestimate of the ocean surface heating could lead to an overestimate in water mass transformation toward water of lower density. As a consequence, the whole water mass transformation annual cycle could be modified. Thus taking into account this penetration of the solar radiation in the prognostic model, as well as in the diagnosis of water mass formation, is of primary importance.

[3] Water mass formation is classically diagnosed from the surface heat flux, following the method introduced by *Walin* [1982] and later extended by *Tziperman* [1986], who also considered freshwater flux. This approach based on surface fluxes provides an estimated upper boundary for water mass formation which can be significantly reduced by diffusion processes in the upper ocean [e.g., *Tziperman*, 1986]. Hence *Marshall et al.* [1993] later introduced a refined diagnosis which allows the computation of subduction rates across a control surface below the mixed layer. The penetration of solar radiation into the ocean subsurface water was not taken into account in these calculations. The inclusion of this penetration factor in the diagnosis has been achieved only recently, by *Iudicone et al.* [2008] who studied its impact in the tropics and in the Southern Ocean using an ocean general circulation model (OGCM). They

[1] Laboratoire d'Océanographie et de Climatologie - Expérimentation et Applications Numériques, LOCEAN/IPSL (previously LODYC), Paris, France.
[2] Laboratory of Biological Oceanography, Stazione Zoologica, SZN, Naples, Italy.
[3] Now at COAPS, Florida State University, Tallahassee, Florida, USA.

0148-0227/08/2007JC004606

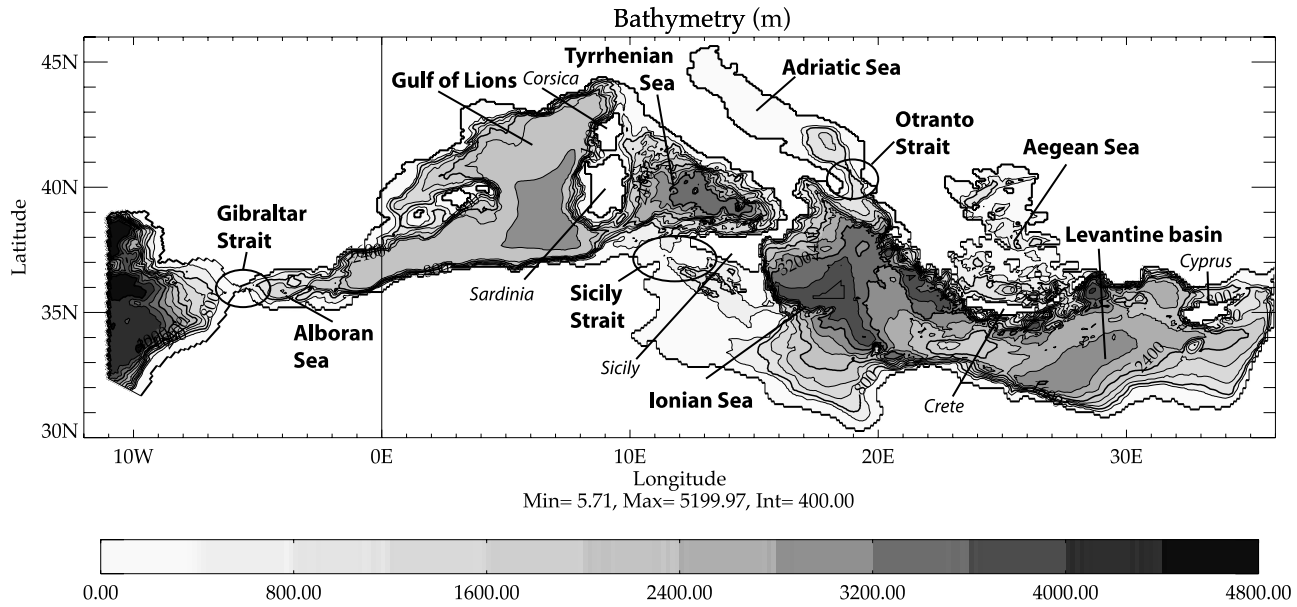

Figure 1. Bathymetry of the MED8 model, with isobath intervals of 400 m. The main locations cited in the text are also displayed on the figure.

found that at global scale the classical method overestimates the seasonal cycle of the water masses transformation by a factor close to 100%.

[4] The purpose of our study was to present revised estimates of Mediterranean water mass formation and mixing and to determine the effect of the penetrative solar radiation on the diagnosis of water mass formation in the Mediterranean Sea, using the output of an ocean model including this parameterization. In this context, the choice of the Mediterranean Sea was particularly relevant, since this semi-enclosed sea has its own specific thermohaline circulation [*Wust*, 1961; *Lacombe and Tchernia*, 1972; *Lascaratos et al.*, 1999]. This thermohaline circulation can be thought of as a progressive transformation of the Atlantic surface inflow, under atmospheric forcing into intermediate and deep water. This transformation occurs in a few locations and feeds the Mediterranean outflow through the Strait of Gibraltar. The yearly transformation cycle has been estimated by *Tziperman and Speer* [1994], who applied the *Walin* [1982] and *Tziperman* [1986] methods to climatological data. They found that the surface heat flux is mainly responsible for the formation of water of maximal and minimal density and for the destruction of water of intermediate density, with annual formation rates in the range [−4 Sv, 2 Sv]. Water mass transformation is counterbalanced by mixing.

[5] The present work was to provide a refined diagnosis of water mass formation rates in the Mediterranean Sea, based on the analysis of numerical simulations of the whole Mediterranean Sea. To do so, we introduced a parameterization of the penetrating solar radiation into the Tziperman and Speer diagnostics. Besides, we quantified the influence of the introduction of a penetrative solar radiation flux into this diagnosis and we established water mass budgets in the mixed layer of the ocean and below the mixed layer.

[6] This paper is organized as follows. In section 2, we describe the oceanic numerical model used in our study. Section 3 covers the description of the atmospheric forcing and a validation of the simulation. Section 4 covers: the revised method for the diagnosis of water mass transformation, as well as a comparison with the "classical" diagnosis [e.g., *Tziperman and Speer*, 1994]; the revised estimation of the mixing of water masses and the annual and the seasonal budgets during spring and summer, when the impact of the penetrative solar radiation is maximal; and a detailed budget of the water masses in the mixed layer and below it. Results are discussed in section 5 (Conclusions).

2. Model Description

[7] The numerical model, hereafter referred to as MED8, encompasses all the Mediterranean basin and has a resolution of 1/8° for longitude and 1/8° cosϕ for latitude. MED8 is one of the Mediterranean configurations of the oceanic model OPA [*Madec et al.*, 1998]. This configuration was derived from the MED16 configuration of the French MERCATOR project [*Drillet et al.*, 2000; *Siefridt et al.*, 2002; *Béranger et al.*, 2004]. The model domain extends from 29°N to 46°N latitude and from 12°W to 38°E longitude, thus including part of the Atlantic Ocean (Gulf of Cadiz; Figure 1). The latter region was modeled as a buffer zone, with a decreasing 3-D relaxation to the MED-ATLAS II climatology [*MEDAR/MEDATLAS Group*, 2002] from the western boundary to Gibraltar. Partial step for bathymetric modeling has been implemented [*Pacanowski and Gnanadesikan*, 1998], which greatly improves the representation of the circulation. The vertical grid has 43 levels with vertical spacing varying from 6 m at the sea surface down to a depth of 200 m. Viscosity and diffusive terms were modeled with a bi-Laplacian in the horizontal with diffusivity and viscosity coefficients equal to -2.5×10^{10} m^4 s^{-1}.

[8] Vertical eddy diffusivity and viscosity were computed from a level 1.5 turbulent closure scheme [*Blanke and*

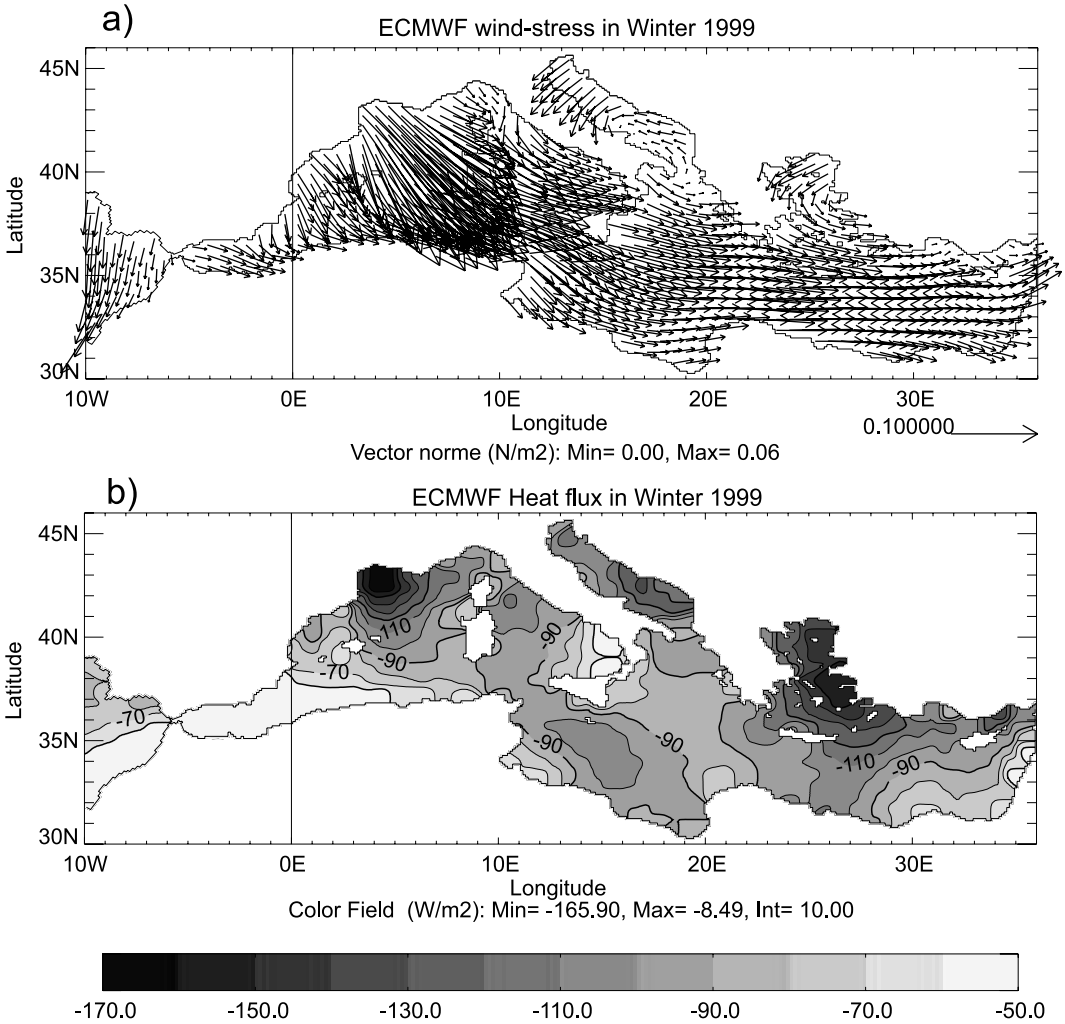

Figure 2. ECMWF atmospheric forcing averaged over winter 1999: (a) the wind stress (in N m^{-2}) is represented by *arrows,* (b) heat flux in W m^{-2}; positive values indicate heat flux from the atmosphere to the ocean.

Delecluse, 1993], with a background value of 1×10^{-5} m^2 s^{-1} for both vertical viscosity and diffusivity. A "Monotonic Upstream-centered Scheme for Conservation Laws" was used as an advection scheme for tracers [*Lévy et al.*, 2001]. Note that simulations were performed within the rigid-lid approximation. The initial temperature and salinity fields were derived from the MEDATLAS II monthly climatology [*MEDAR/MEDATLAS Group*, 2002]. Wind stress data and air–sea fluxes were obtained from the European Centre for Medium Range Weather Forecasting (ECMWF). Solar radiation flux is a function of depth, as described in section 4.1.1. Heat flux was applied at the model surface using the correction method [*Barnier et al.*, 1995], which combines a climatological record of the atmospheric heat flux and a retroaction term modeled as a relaxation term. In our study, this term includes a variable relaxation coefficient ranging from -10 W m^{-2} K^{-1} in winter to -40 W m^{-2} K^{-1} in summer and relaxes the modeled SST toward the SST of *Reynolds* [1988]. The resulting heat flux is referred to as the net heat flux. Freshwater fluxes (evaporation, precipitation and river runoffs) were applied as a virtual salt flux that includes a relaxation term equivalent to -40 W m^{-2} K^{-1}, constant over the year. A UNESCO monthly climatology of 31 river runoffs based on the RivDis database was implemented including the Black Sea outflow to the Aegean Sea.

3. Validation of the Simulation

3.1. ECMWF Atmospheric Forcing

[9] A specific feature of the atmospheric circulation over the Mediterranean Sea, due to the complex orography, is the presence of local winds, such as the Mistral [Gulf of Lions; *Madec et al.*, 1996] or the Etesian wind (Aegean Sea). The result is that only high-resolution atmospheric models are able to reproduce these local features [*Horton et al.*, 1994]. We considered here the high-resolution ECMWF analysis (equivalent to $0.5° \times 0.5°$) which allows a good representation of local winds over the period 1998–2002. An example of these local winds is shown in Figure 2 where the winter average of the wind stress field is displayed. In the western basin, the strong local wind blowing southeastward, called the Mistral, contributes to deep water formation [*MEDOC Group*, 1970; *Madec et al.*, 1996]. This wind is

Table 1. Yearly Averaged Heat Flux and Equivalent Freshwater Flux for the Whole Mediterranean Basin[a]

	Heat Flux, W m^{-2}	E-P-R Flux, mm d^{-1}
ECMWF-atmosphere	−28.3 ± 123.4	1.67 ± 1.02
ECMWF-ocean	−2.79 ± 130.9	0.64 ± 1.22

[a]ECMWF-ocean includes the atmospheric forcing provided by the atmospheric ECMWF model plus the river run-off(ECMWF-atmosphere) and the restoration term for the heat flux or the relaxation term for the equivalent freshwater flux.

well represented in the high-resolution model (Figure 2a). In the eastern basin, the cold and dry Etesian wind plays a major role. Its cyclonic circulation, blowing from the northeast, north of the Aegean Sea, and then from the northwest in the Levantine basin, is present in the ECMWF output.

[10] Statistics of the total heat flux and freshwater budget are given in Table 1. The sign convention for heat flux is positive from the atmosphere to the ocean. Note that both intrinsic and real values, i.e., including the restoring term, are displayed. In the model, the yearly mean surface heat flux (atmospheric flux plus retroaction term) was −2.79 W m^{-2}. This is consistent with observations [*Béthoux*, 1979; *MacDonald et al.*, 1994] that indicate a heat loss from the Mediterranean Sea to the atmosphere between 3 and 7 W m^{-2} (heat advected through the Strait of Gibraltar ensures conservation of heat). Similarly, the equivalent freshwater flux at the atmosphere–ocean interface (evaporation minus precipitation minus runoff) is underestimated by the model. The average model value of 0.64 mm d^{-1} over the Mediterranean basin, is significantly smaller than the 2.5 mm d^{-1} inferred from observations [*Garrett et al.*, 1993].

[11] To get a deeper understanding of the spatial distribution of the total heat flux during the key wintertime period, a map is given in Figure 2b. Higher values for the heat loss were obtained in the main regions of convection, namely in the Levantine basin, in the Adriatic Sea and in the Aegean Sea for the eastern basin, as described by *Lascaratos et al.* [1999], and in the Gulf of Lions for the western basin [*MEDOC Group*, 1970]. These values were in agreement with observations: ∼−100 W m^{-2} in the Adriatic Sea [*Artegiani et al.*, 1997]; and ∼−110 W m^{-2} in the Gulf of Lions [*Mertens and Schott*, 1998], which was of particular relevance for our simulations, since a high heat loss is necessary to drive the preconditioning phase of the convection [e.g., *Schott and Leaman*, 1991, for the Gulf of Lions].

3.2. Oceanic Circulation

[12] The oceanic model was forced during 12 years with three cycles of the four years (1998–2002) of the high-resolution atmospheric model (ECMWF). The kinetic energy reached a steady state after 8 years. These first 8 years were considered as the spin-up of the model. The initial state was inferred from the MEDATLAS II climatology [*MEDAR/MEDATLAS Group*, 2002]. The simulation was started in August, when the surface layer is strongly stratified, and the atmospheric forcing is weak. This ensures that the effects of mixing were weak at the beginning of the spin-up period. A brief description of the oceanic circulation is given in the following subsections. The main purpose is to show the ability of the model to reproduce intermediate and deep water formation.

3.2.1. Surface Currents

[13] The surface current field is shown in Figure 3a. In the western basin, the Atlantic inflow first forms the anticylonic Alboran gyre, east of the Strait of Gibraltar, as described by *Vargas-Yañez et al.* [2000]. Then, this inflow flows eastward along the North African coast forming the Algerian Current. In the Tyrrhenian Sea, between Sardinia and Italy, the Atlantic water, now called Modified Atlantic Water (MAW), splits into two branches: the first one flows through the Strait of Sicily and enters the eastern basin, while the second one flows north of Sicily into the Tyrrhenian Sea [*Astraldi et al.*, 2002]. This latter branch then moves along the Italian coast to the French coast and feeds the "Liguro-Provençal" Current, in agreement with *Millot* [1999].

[14] In the Strait of Sicily, the eastward branch of the MAW separates into two branches as it enters the Ionian Sea, as shown by *Béranger et al.* [2004]. One of these branches follows the North African coast, while the other one follows a more sinuous path in the northern part of the Ionian Sea, becoming the Atlantic–Ionian Stream [*Robinson et al.*, 1999]. In the Southern Adriatic Sea, surface water originating in the eastern basin flows through the Strait of Otranto and mixes with the Adriatic water in the cyclonic gyre in the southern part of the basin [*Poulain*, 2001]. In the Levantine basin, the cyclonic circulation along the Middle-East coast is in agreement with that described by *Alhammoud et al.* [2005].

3.2.2. Mixed-Layer Depth

[15] A snapshot of the maximum mixed-layer depth in February is given in Figure 3b. The mixed-layer depth is defined as the depth at which the potential density exceeds the surface value by 0.01 kg m^{-3}. This parameter is a good indicator of the ability of the model to represent the formation of intermediate and deep waters.

[16] Four main sites of water mass formation were thus identified: the Gulf of Lions, in the western basin; the Adriatic Sea; the Levantine basin; and the Aegean Sea, in the eastern basin. In the model, the mixed-layer depth has a significant interannual variation. In the Gulf of Lions, mixed-layer depth varied from 800 to 2700 m during the simulation (Figure 3b). In the Levantine basin, intermediate water was formed at a depth between 400 and 500 m. In the Adriatic Sea, the mixed-layer often went below 900 m, down to 1100 m at the end of the simulation. Finally, in the western part of the Cretan Sea, some Cretan Intermediate Water was formed, with a mixed-layer depth of 800 m (Figure 3b).

[17] These results compared quite well with observations. The mixed-layer depth in the Gulf of Lions, where the Western Mediterranean Deep Water (WMDW, potential density $\rho > 29.05$ kg m^{-3}) forms, can reach 2700 m (bottom of the basin) with a significant interannual variation [*MEDOC Group*, 1970]. At intermediate depth, Western Intermediate Water (WIW) also forms, between 150 and 250 m, with a potential density greater than 28.8 kg m^{-3} [*Fuda et al.*, 2000]. In the eastern basin, the mixed-layer depth can exceed 1000 m in the Adriatic Sea, where the Eastern Mediterranean Deep Water (EMDW) is formed, with potential density greater than 29.1 kg m^{-3} [*Roether*

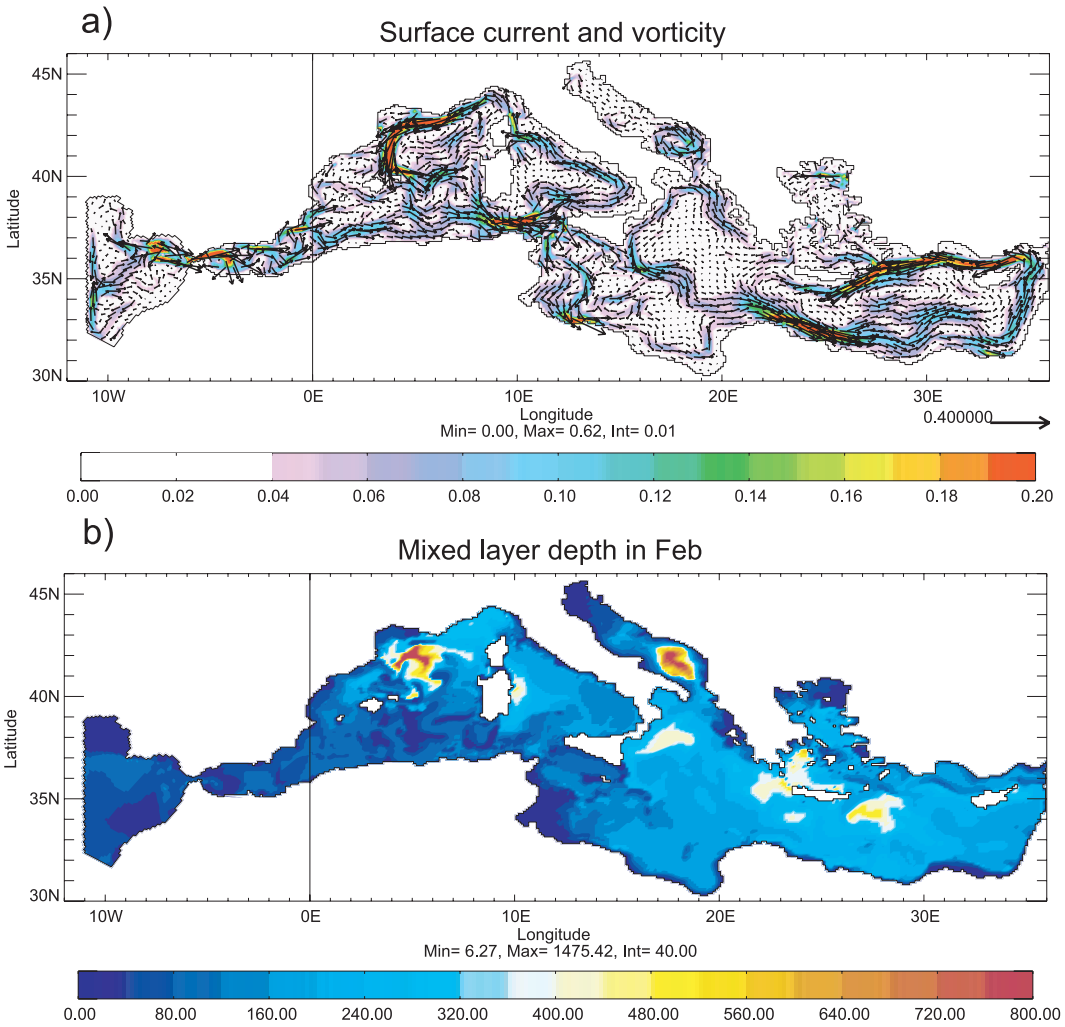

Figure 3. (a) Mean surface circulation in winter: the relative vorticity (s^{-1}) is represented by a *color-scale* and the current (m s^{-1}) is indicated by the *arrows*. (b) Snapshot of maximum mixed-layer depth (m) in February of year 10.

and Schlitzer, 1991; *Vilibic and Orlic*, 2002]. In the Levantine Basin, the mixed-layer depth can reach about 500 m where Levantine IntermediateWater (LIW) was formed ($28.9 < \rho < 29.1$ kg m^{-3} [*Roether et al.*, 1998]). This depth can exceed 1000 m when Levantine Deep Water is formed [*Gertman et al.*, 1994]. In the Aegean Sea, Cretan Intermediate Water and Cretan Deep Water (above 2500 m) forms intermittently created, as described by *Theocharis et al.* [2002].

4. Water Mass Formation

4.1. Revised Tziperman-Speer Method

[18] Since the prognostic model MED8 includes the penetration of the solar radiation, our revised diagnosis takes into account this parameterization.

4.1.1. Penetrative Solar Radiation

[19] The vertical penetration of the solar radiation is classically described by decreasing exponential functions versus depth. This decrease obviously depends on the characteristics of the water, mainly the concentration of pigments and particles in suspension [*Morel and Antoine*, 1994; *Frouin and Iacobellis*, 2002]. In the numerical model MED8, this effect is taken into account by using a depth dependency of the solar radiation flux given by the following equation (see Figure 4) which approximately models the spectral dependence of the attenuation on depth:

$$Q_{sol}(x,y,z) = Q_0(x,y)\left[\mathrm{Re}^{-\frac{z}{\xi_1}} + (1-R)e^{-\frac{z}{\xi_2}}\right] \qquad (1)$$

Where $Q_0(x, y)$ is the solar radiation flux across the sea surface at each point. The parameters $\xi_1 = 0.35$ m, $\xi_2 = 23$ m and R = 0.58 correspond to a Type I water in the classification of *Jerlov* [1968].

[20] Prior to a detailed analysis, it is useful to get a first insight into the impact of the penetrative solar radiation on water mass formation, in the MED8 model. This impact depends on the stratification of the upper layer which determines the density range of the seawater influenced by the penetrative solar radiation. This effect is clearly evident when the vertical profiles of the seasonally averaged potential density (reference in surface) and that of the solar heat flux are compared (Figure 4a). Note that each season

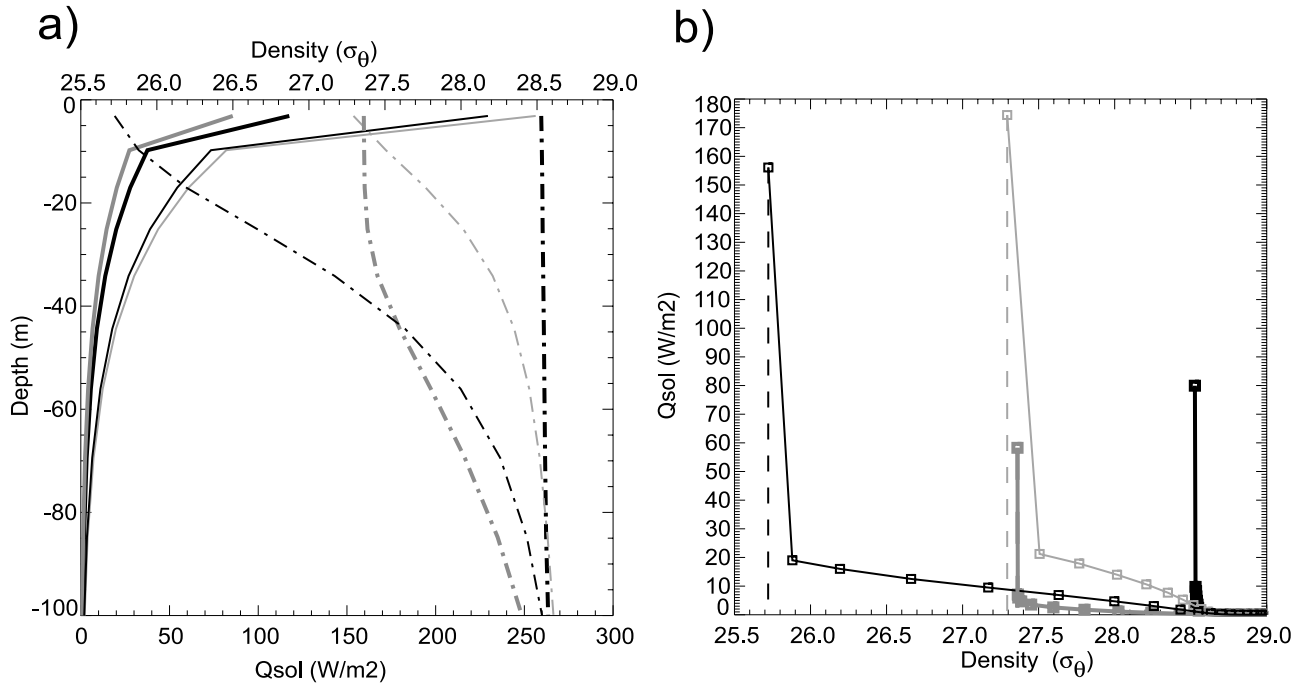

Figure 4. (a) Mean seasonal potential density profiles (in kg m^{-3}; *dash-dotted lines*) and penetrative solar radiation (Q_{sol} in W m^{-2}; *full lines*) versus depth for the whole Mediterranean Sea. Each season is color-coded so that winter (January–February–March) corresponds to the *thick black line*, autumn to the *thick grey line*, summer to the *thin black line*, spring to the *thin light-grey line*; (b) Penetrative solar radiation versus mean seasonal potential density, with the same color-code as in Figure 4a.

corresponds to three full months: winter is January, February, March; spring is April, May, June; summer is July, August, September; and autumn is October, November, December. One can easily see that the widest density range corresponds to the solar heat flux in spring and summer. The strongest density variations occurred during these two seasons in the first 60 m of the water column, for which the solar heat flux was significant (160 W m^{-2} at the surface to 5 W m^{-2} at 60 m depth, in summer, and 170 W m^{-2} at the surface to 5 W m^{-2} at 60 m depth, in spring). For a quantitative characterization of this effect, the solar heat flux received per density range averaged over the Mediterranean basin is given in Figure 4b, for the four seasons. The range of potential density influenced by the solar radiation is 2.8 kg m^{-3}, in summer, and 1.2 kg m^{-3}, in spring, whereas this range tends to zero in autumn and winter, owing to the almost insignificant stratification in the first 60 m due to mixing.

4.1.2. The Revised Diagnosis Computation

[21] An upper limit for water mass formation can be derived from the buoyancy forcing. The method was developed by *Walin* [1982] who computed the net volume flux per density interval from the surface heat flux. Later *Tziperman* [1986] included the surface water flux, while *Nurser et al.* [1999] and *Marshall et al.* [1993] added the diffusive diapycnal fluxes. Finally, a generalized approach was proposed by *Iudicone et al.* [2008] that includes the penetrative character of the solar radiative flux and the use of a neutral density framework. In the following we use the method presented by *Iudicone et al.* [2008]:

[22] The buoyancy flux per unit area, B_m, is computed as follows:

$$B_m = g\frac{\alpha}{C_p}Q_{tot} - g\beta S(E-P) \tag{2}$$

where *E-P* is the net water flux (evaporation–precipitation–runoff (in kg m^{-2} s^{-1})) acting at the sea surface, S is the surface salinity, C_p the specific heat (equal to 4000 J kg^{-1} K^{-1}), $\alpha = -\frac{1}{\rho_0}\frac{\partial\rho}{\partial\vartheta}$ the thermal expansion coefficient and $\beta = \frac{1}{\rho_0}\frac{\partial\rho}{\partial S}$ the saline contraction coefficient. Q_{tot} is the total net heat flux into the ocean (in W m^{-2}). Q_{tot} is decomposed into a surface heat flux (longwave + latent + sensible heat flux + restoring) denoted Q_{nsol} and a heat flux acting in the mass of fluid, Q_{sol}. Thus Q_{tot} can be written as:

$$Q_{tot}(x,y,z) = Q_{nsol}(x,y)\delta_{z=0} + Q_{sol}(x,y,z) \tag{3}$$

where $\boldsymbol{\delta_{z=0}}$ is the Dirac function equal to 1 at z = 0, and 0 elsewhere.

[23] Since the prognostic model MED8 includes the penetration of the solar radiation, our revised diagnosis takes it into account.

[24] The mass transformation rate $\Phi(\rho)$ for a water of potential density ρ within $[\rho - \frac{1}{2}\Delta\rho,\ \rho + \frac{1}{2}\Delta\rho]$ is inferred from the buoyancy flux (equation (2)) integrated over a volume bounded by the density surfaces $\rho - \frac{1}{2}\Delta\rho$ and $\rho + \frac{1}{2}\Delta\rho$ and over a duration T (Figure 5). It is driven first by surface effects due to Q_{nsol} and E – P acting on the area A bounded by the outcropping density surfaces $\rho - \frac{1}{2}\Delta\rho$ and $\rho + \frac{1}{2}\Delta\rho$ and secondly by volume effects due to Q_{sol} acting on a volume V bounded by the density surfaces $\rho - \frac{1}{2}\Delta\rho$ and $\rho + \frac{1}{2}\Delta\rho$ (see Figure 5). The expression of the transformation

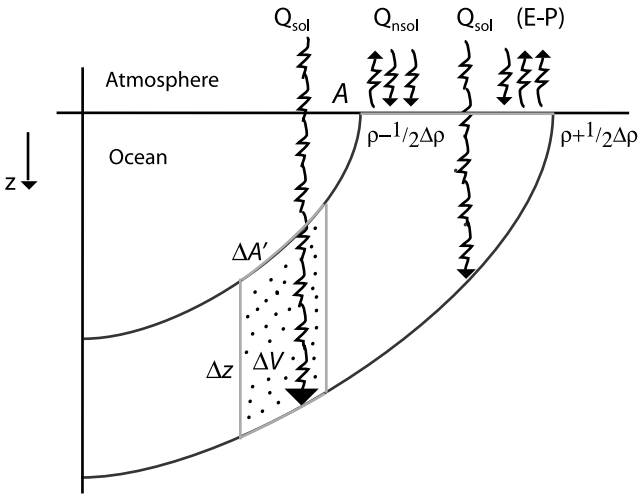

Figure 5. Scheme of the surface forcing effects on a density layer (dotted area) between $\rho - \frac{1}{2}\Delta\rho$ and $\rho + \frac{1}{2}\Delta\rho$. $\boldsymbol{Q_{nsol}}$ is the nonsolar heat flux, $E - P$ is the freshwater flux and $\boldsymbol{Q_{sol}}$ is the penetrative solar radiation.

rate is given by the following equation (Π corresponding to the top-hat function equal to 1 for $\rho - \frac{1}{2}\Delta\rho < \rho < \rho + \frac{1}{2}\Delta\rho$, and zero elsewhere):

$$\Phi(\rho) = \frac{1}{T}\int_0^T dt \iint_A \left[\frac{\alpha}{C_p} Q_{nsol} - \beta S(E-P)\right] \cdot \Pi\left(\rho - \frac{1}{2}\Delta\rho, \rho + \frac{1}{2}\Delta\rho\right) dA + \frac{1}{T}\int_0^T dt \iint_{A'} \frac{\alpha}{C_p}\int_z \frac{\partial Q_{sol}(x,y,z)}{\partial z} \cdot \Pi\left(\rho - \frac{1}{2}\Delta\rho, \rho + \frac{1}{2}\Delta\rho\right) dz dA' \quad (4)$$

As in the work of *Tziperman and Speer* [1994] let us defined a volume transformation rate per density interval as $F(\rho) = \lim(\Delta\rho \to 0)\frac{\Phi(\rho)}{\Delta\rho}$. The quantity F that is expressed in Sv (1 Sv = 10^6 m^3 s^{-1}), is a more familiar quantity than the transformation rate Φ. Note that the difference with previous methods consists in the inclusion of the solar irradiance as a 3-D term in (4).

[25] Equation (4) is discretized on the grid of the numerical model, with volume grid cells $\Delta x \times \Delta y \times \Delta z$, with an elementary density interval of width $\Delta\rho$ and for a duration of NΔt. Only the term that includes the solar radiation flux is discretized on the 3-D grid of the numerical model; the others terms are only discretized on the horizontal grid. One then gets the revised volume transformation rate per density interval, F as:

$$F(\rho) = \frac{1}{N\Delta t}\frac{1}{\Delta\rho}\sum_{n=1}^{N}\Delta t \sum_{i,j}\Delta x\Delta y\left[\frac{\alpha}{C_p} Q_{nsol} - \beta S(E-P)\right] \cdot \Pi\left(\rho - \frac{1}{2}\Delta\rho, \rho + \frac{1}{2}\Delta\rho\right) + \frac{1}{N\Delta t}\frac{1}{\Delta\rho}\sum_{n=1}^{N}\Delta t \sum_{i,j,k}\Delta x\Delta y\Delta z\left[\frac{\alpha}{C_p}\cdot\frac{\partial Q_{sol}(x,y,z)}{\partial z}\right] \cdot \Pi\left(\rho - \frac{1}{2}\Delta\rho, \rho + \frac{1}{2}\Delta\rho\right) \quad (5)$$

The quantity F corresponds to that defined by equation (4) in the work of *Tziperman and Speer* [1994] with the same sign convention (positive for a transformation from high to low densities) to facilitate comparisons.

4.1.3. Impact of the Penetrative Solar Radiation in the Diagnosis of Water Mass Formation

[26] The purpose of this section is to provide a first characterization of the impact of the penetrative solar radiation in the diagnosis of water mass formation. For that, as in the study by *Tziperman and Speer* [1994], we estimated the annual volume transformation rate F (Figure 6a), computed over the basin, using both the "classical" diagnosis and the "revised" diagnosis (equation (5)). For this study, we chose a potential density increment $\Delta\rho = 0.12$ kg m^{-3} and a Δt of 1 month as by *Tziperman and Speer* [1994]. We present here the analysis of year 10 of the simulation, whose behavior is close to that of the other years. The mean annual transformation rate per density interval $\Delta\rho$ (i.e., $F(\rho)$ expressed in Sv) is shown in Figure 6.

[27] The annual transformation rate computed with the classical method (grey line in Figures 6a, 6c, and 6e) is similar in shape to that obtained by *Tziperman and Speer* [1994, Figure 1] but their values are slightly lower than ours, which can be attributed to the fact that they analyzed climatological data and not model data as in this study. The transformation rate presents a maximum at $\sigma_\theta = 26$ kg m^{-3} corresponding to a flux of about 3 Sv flowing from greater densities to lower ones. It is minimum at $\sigma_\theta = 28.7$ kg m^{-3}, corresponding to about 6 Sv of light waters transforming to greater densities. Similarly, we found about 1 Sv of intermediate and dense waters (WIW, LIW and WMDW) formed in the western basin (Figure 6c) and 4.5 Sv (LIW and EMDW) formed in the eastern Mediterranean basin (Figure 6e), as by *Tziperman and Speer* [1994, Figures 2 and 3]. Finally, note that from the analysis above, it results that, in the Mediterranean Sea, the main part of the transformations takes place in the eastern basin.

[28] The first striking effect of the use of a penetrative solar radiation in the diagnosis is a reduction in the amplitude of water mass transformation with an unchanged shape. This is clearly seen in the yearly averaged transformation rates shown in Figures 6a, 6c, and 6e. The annual cycle is significantly reduced when the penetrative solar radiation is taken into account, with an amplitude of about 5.2 Sv, to be compared with the classical diagnosis range of 9 Sv for the whole Mediterranean Sea (Figure 6a). The most important difference concerns the eastern basin, with a range of 4.2 Sv in the seasonal cycle, to be compared to a classical diagnosis range of 6.4 Sv. Transformation rates of deep and intermediate waters change to a lesser extent, except that of LIW which is decreased by about 20% (Figures 6c and 6e). The impact of the new estimate concerns mostly the MAW. The seasonally averaged transformation rates are presented in Figures 6b, 6d, and 6f.

[29] As expected, the two methods provide almost identical diagnoses in autumn and winter (Figures 6b, 6d, and 6f). This results from the fact that the mixed layer was deeper than the penetration depth of the solar radiation, as underlined in section 4.1.1. In contrast, major changes are observed in spring and summer (Figures 6b, 6d, and 6f). With the revised method, a larger density range is influenced by the penetrative solar radiation due to the shallow-

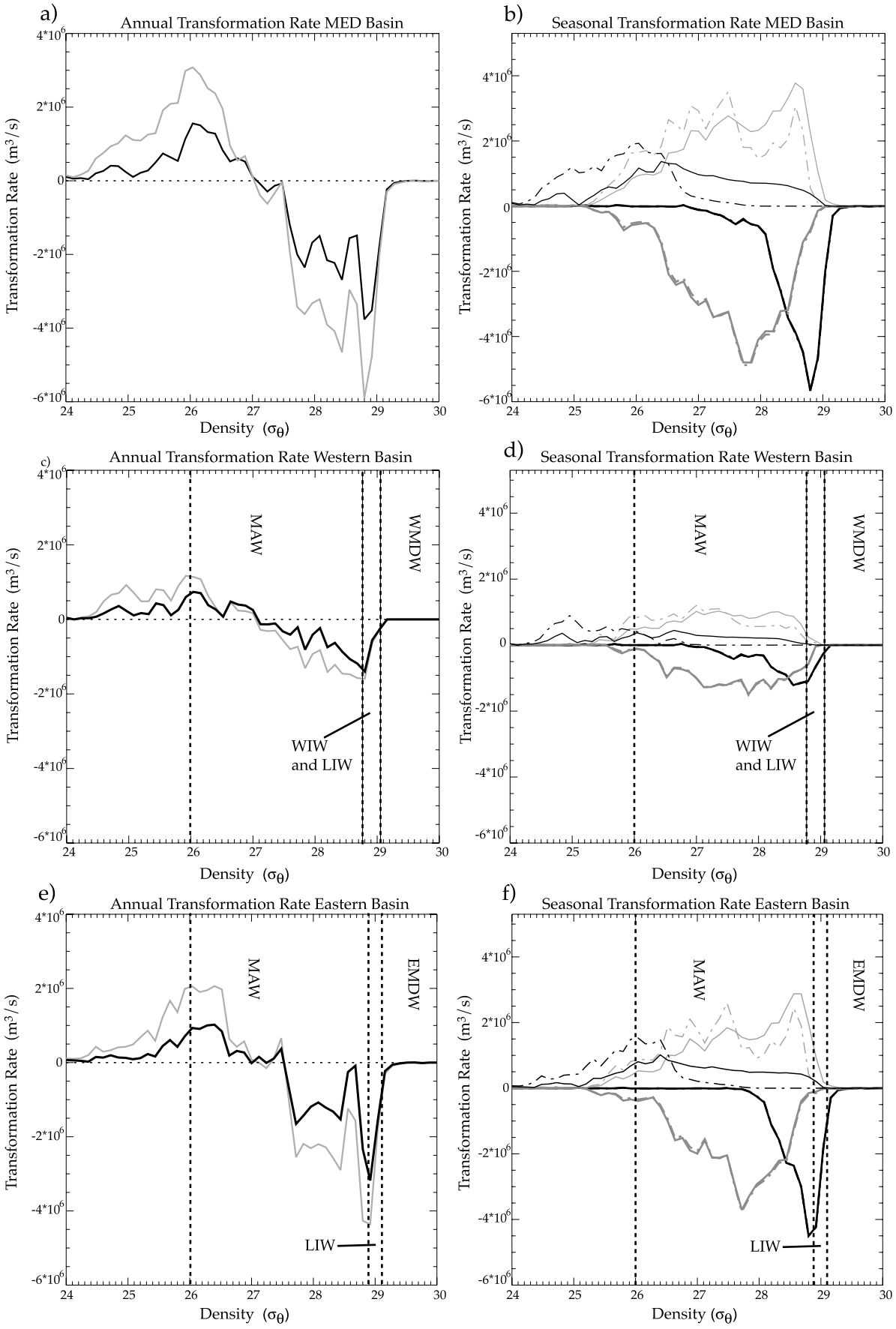
a)
Annual Transformation Rate MED Basin
b)
Seasonal Transformation Rate MED Basin
c)
Annual Transformation Rate Western Basin
d)
Seasonal Transformation Rate Western Basin
e)
Annual Transformation Rate Eastern Basin
f)
Seasonal Transformation Rate Eastern Basin
Transformation Rate (m3/s)
Density (σθ)
MAW
WMDW
EMDW
WIW
and LIW
LIW

Figure 6

ness of the mixed layer. This has two main consequences. First a weaker transformation rate is obtained for the lowest densities, i.e., surface waters, due to a reduced solar heating contribution. Secondly, it highlights the contribution of the penetrative solar radiation to the transformation of fairly high-density water into lighter water, due to a reduced absorption of solar radiation in the mixed layer. More precisely, in spring the transformation rate is reduced for potential densities less than $\sigma_\theta = 27.6$ kg m^{-3} and increased for higher densities, up to 29 kg m^{-3}. Also, the upper boundary of the density range influenced by the solar radiation flux is slightly shifted, from 28.8 to 29 kg m^{-3}, during these seasons in the eastern basin, showing the partial destruction of the LIW formed in winter (Figure 6f). In the western basin, a more important quantity of WIW and LIW at densities between 28.6 and 29 kg m^{-3} (Figure 6d) is transformed into lighter water. The most important changes concerns the summer season when the solar radiation flux is maximum and the mixed layer at its shallowest. The density range influenced by the solar radiation flux is then much wider, reaching an upper boundary of 28.9 kg m^{-3} in the eastern basin (Figure 6f), to be compared to that of 27.5 kg m^{-3} obtained with the classical method and an upper boundary of 28.7 kg m^{-3} in the western basin (Figure 6) to be compared to that 26.8 kg m^{-3} with the classical method. These high-density waters (basically LIW) are then destroyed in summer. As a consequence of the reduced solar radiation flux with respect to the water of lowest density (surface water and MAW), their transformation rate is reduced. In summary, the main impact of the penetrative solar radiation is to destroy high-density water created during autumn and winter. The rate of destruction reaches 50% of the rate of formation (about 0.2 Sv in summer and about 1.1 Sv in spring; Figure 6b). This change is particularly relevant to the estimation of water mass mixing as discussed in the following. Indeed, using the classical method for determining water mass formation, the high-density water masses formed in autumn and winter were ''seen'' to be destroyed only through mixing, if one assumes zero annual variation in water volume in the Mediterranean Sea.

4.2. Revised Estimate of Mixing

[30] The analysis of the life cycle of water masses was conducted on the basis of volume budgets of water contained between two isopycnals. To this end we used the equation of conservation of water volume established by *Nurser et al.* [1999] [see also *Large and Nurser*, 2001], which is valid under the Boussinesq approximation and for an incompressible fluid. The time derivative of a water volume of potential density ρ between the isopycnals $\rho - 1/2\Delta\rho$ and $\rho + 1/2\Delta\rho$ with open boundaries is given by:

$$\left(\frac{\partial \Delta V}{\partial t} + \Delta\psi\right) = \Gamma\left(\rho + \frac{1}{2}\Delta\rho\right) - \Gamma\left(\rho - \frac{1}{2}\Delta\rho\right) \qquad (6)$$

where $\frac{\partial \Delta V}{\partial t}$ is the time variation in the volume between the isopycnes $\rho - 1/2\Delta\rho$ and $\rho + 1/2\Delta\rho$, $\Delta\psi$ is the volume flux of fluid (advective flux) exiting the domain, $\Gamma(\rho)$ a cross-isopycnal volume flux $\Gamma = F + \frac{\partial D_{diff}}{\partial \rho}$ in which $F(\rho)$ is the volume transformation rate from high to low densities computed from equation (5) and D_{diff} the diapycnal density flux, Volume variations resulting from mixing (i.e., D_{diff}) can thus be inferred indirectly from the volume budget (equation (6)). For the sake of simplicity, we analyzed the diapycnal transport across ρ, namely the volume budget for water lighter than ρ as deduced from the integration in ρ of equation (6). Let us now integrate equation (6) with respect to density intervals. We obtain a budget equation for density of the form:

$$\left(\overline{\frac{\partial \Delta V}{\partial t}} + \overline{\Delta\psi}\right) = \Gamma(\rho) \qquad (7)$$

where $\overline{\frac{\partial \Delta V}{\partial t}}$ is equal to $\frac{1}{\rho - \rho_{\min}} \int \frac{\partial \Delta V}{\partial t} d\rho$

$\overline{\Delta\psi}$ is equal to $\frac{1}{\rho - \rho_{\min}} \int \Delta\psi d\rho$

and $\rho_{\min}$ is the minimum density of the Mediterranean water under consideration.

4.2.1. Annual Water-Volume Budget

[31] The annual volume budgets per density interval integrated over the whole Mediterranean Sea (from equation (7)), are displayed in Figures 7a, 7b, and 7c. The budgets are computed for basins represented as boxes with open boundaries. For the Mediterranean Sea budget, the box includes the whole basin east of the Strait of Gibraltar (Figure 7a). For the western basin, the control volume occupies the part of the Mediterranean Sea lying between the Strait of Gibraltar and the Strait of Sicily (Figure 7b). Finally, the eastern basin is bounded by the Strait of Sicily (Figure 7c).

[32] These volume budgets revealed two predominant, mostly counteracting, terms: the transformation rate (in-

Figure 6. (a), (c), and (e): Annual water mass transformation rate (F(ρ) in m^3 s^{-1} integrated over the whole density range versus density (kg m^{-3}), for year 10 of the simulation: for the whole Mediterranean basin (Figure 6a); for the western Mediterranean basin (Figure 6c); for the eastern Mediterranean basin (Figure 6e); the result for the classical method is represented by a *grey line* and for the revised method, by a *black line*. (b), (d) and (f): Seasonal transformation rate (F(ρ), in m^3 s^{-1}) integrated over the whole density range versus density (kg m^{-3}): for the whole Mediterranean basin (Figure 6b); for the western Mediterranean basin (Figure 6d); for the eastern Mediterranean basin (Figure 6f); the color-code for season is the following: winter in *thick black line*; spring in *thin light-grey line*; summer in *thin black line*; and autumn in *thick grey line*; the classical method is displayed by a *dashed line* and the revised method, with a *continuous line*. The potential density increment is $\Delta\rho = 0.12$ kg m^{-3}. *Vertical dashed lines* bound the density intervals of the different water masses of the basin (for definition see section 3.2.2). *MAW* Modified Atlantic Water; *WMDW* Western Mediterranean Deep Water; *EMDW* Eastern Mediterranean Deep Water; *LIW* Levantine Intermediate Water; *WIW* Western Intermediate Water.

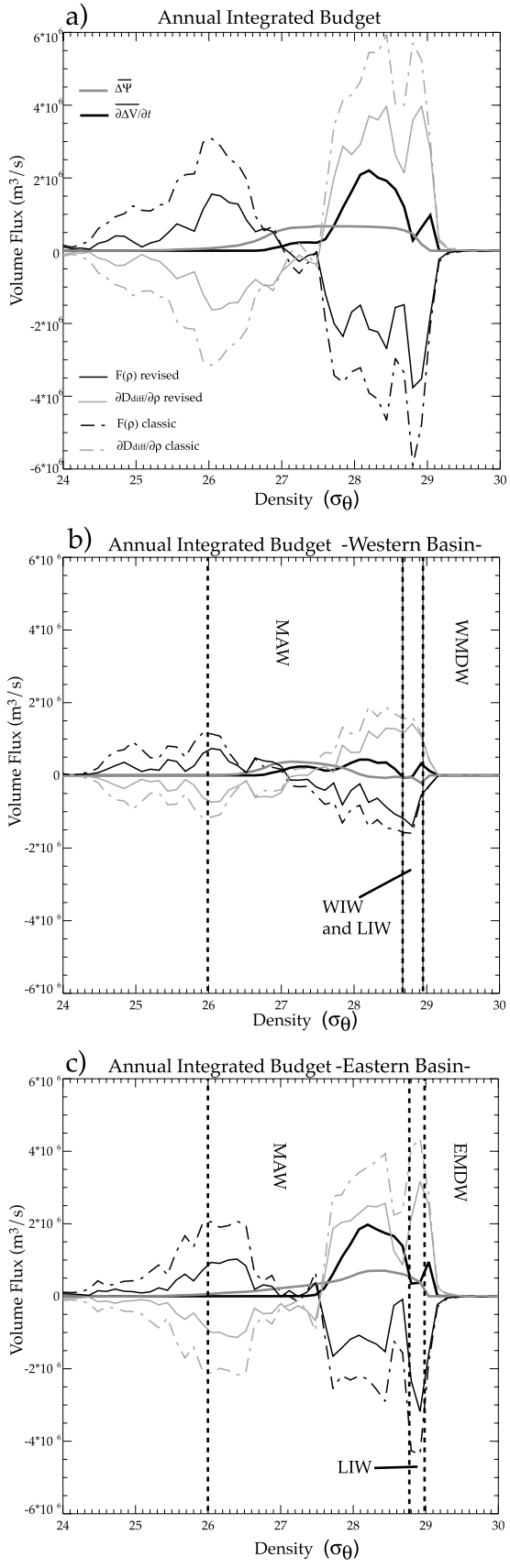

Figure 7. Annual water volume budget versus potential density: (a) for the Mediterranean basin, (b) for the western basin, and (c) for the eastern basin. The different terms of equation (8) integrated over density are displayed: $\overline{\frac{\partial \Delta V}{\partial t}}$, is represented by a *thick black line*, the advection term, $\overline{\Delta \psi}$, by a *thick dark-grey line*, the diapycnal fluxes terms, $\frac{\partial D_{diff}}{\partial \rho}$, by a *thin light-grey line*, and the transformation rate (as in Figure 6), F(ρ), by a *thin black line*. Terms inferred using the revised method are plotted with a *full line*, while those inferred using the classical method are plotted with a *dash-dotted line*. *Vertical dashed lines* mark the density layers of the different water masses of the basin (for definition see Figure 6 and section 3.2.2).

duced by atmospheric fluxes) and the diapycnal fluxes (i.e., mixing). The other terms are indeed much smaller, with an advective flux of about 0.75 Sv corresponding to the Strait of Gibraltar and a negligible volume variation, except for the highest-density water, with a value of about 2 Sv (Figure 7a). The transformation rate (i.e., $F(\rho)$) induced by the heat and freshwater flux is responsible for the formation of waters of minimal and maximal densities that were transformed by mixing into waters of intermediate densities. Conversely, these waters of intermediate densities were destroyed through heat and freshwater fluxes. Since the transformation rate is significantly overestimated by the classical method, revised estimates of diapycnal fluxes were significantly reduced, as shown in Figures 7a, 7b, and 7c.

[33] In the western basin, this overestimation of mixing mostly concerned the density range below σ_θ = 28.7 kg m^{-3}. The transformation of MAW through mixing was overestimated by an amount of 1 Sv namely 30% of its previous value of 2.9 Sv and the volume of surface waters destroyed through mixing was overestimated by 0.5 Sv namely 42% of its previous value and that of the LIW and WIW by 0.5 Sv namely 30% its previous value (Figure 7b). In the eastern basin, transformation of MAW through mixing was overestimated by an amount of 2.2 Sv namely 35% its previous value (Figure 7c). The diapycnal fluxes in the surface water density range were estimated at twice the revised value by the classical method (Figure 7c). In the LIW density range, the transformation rate and the diapycnal fluxes were also overestimated, by about 31% by the classical method. In the EMDW density range, we found similar values with the classical and the revised methods.

4.2.2. Seasonal Water-Volume Budget

[34] Seasonal integrated budgets are given in Figure 8. In autumn and winter the densest water is formed because of surface cooling and evaporation. The net volume variation (time derivative) of this newly formed water is slightly reduced by mixing (Figures 8c and 8d). During these two seasons, the transformation rate remained unchanged if the penetrative solar radiation was taken into account in the diagnosis, as previously mentioned.

[35] In spring the net variation in water volume was characterized by a decrease, for the densest water, of potential density greater than 28.4 kg m^{-3}, and by an increase, for the lightest water, of potential density between

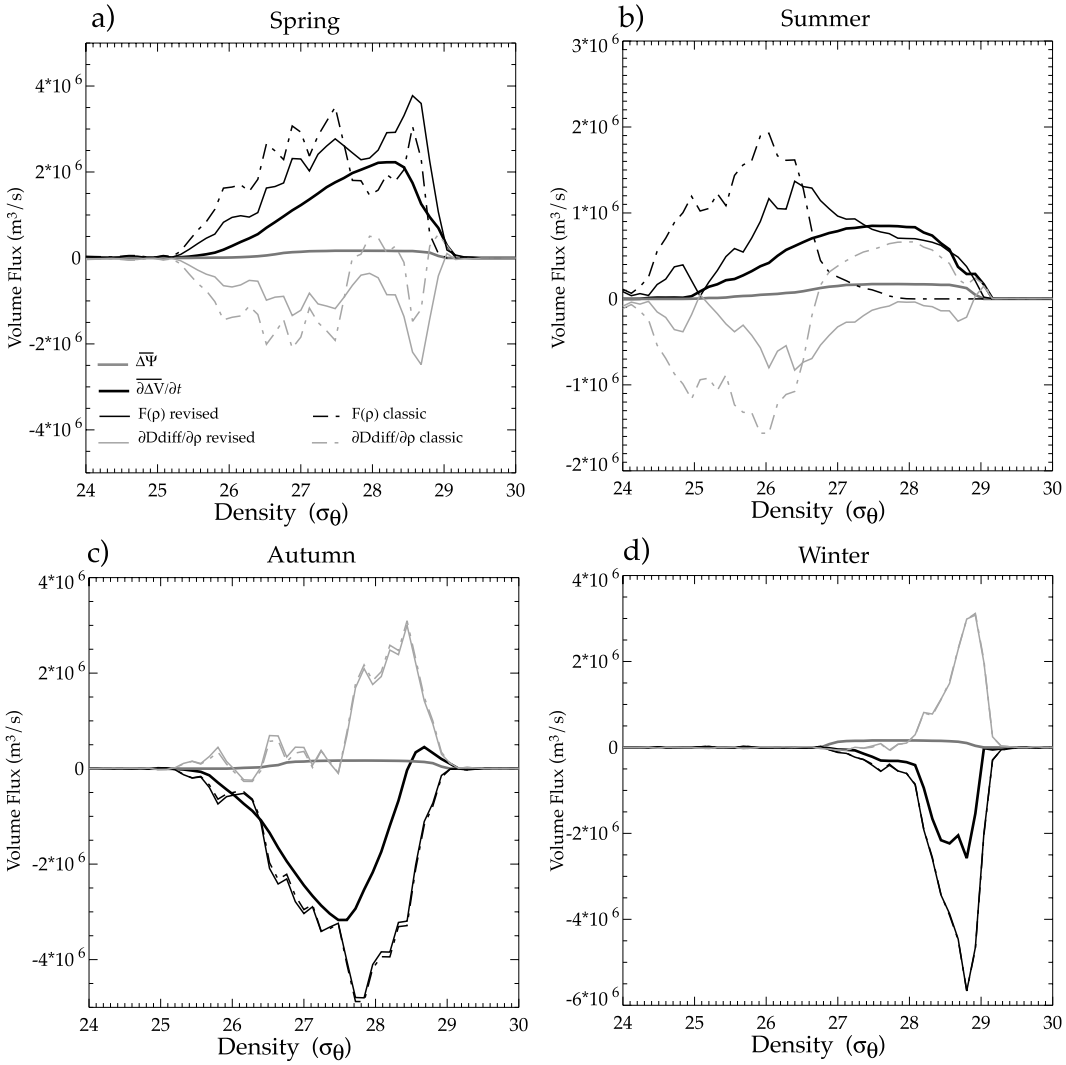

Figure 8. Seasonal water volume budget versus potential density: (a) in spring, (b) in summer, (c) in autumn, and (d) in winter; Color-coded lines as in Figure 7. Positive values of the slope are related to the formation of water masses, negative values, to the destruction of water masses.

25 and 28 kg m^{-3} (Figure 8a). Again both transformation rate and diapycnal fluxes play a counteracting role in this evolution, as detailed above.

[36] In the range σ_θ < 28. kg m^{-3}, the analysis of the revised method showed an overestimation of the budget but the shape of the different curves remains similar.

[37] The main difference appeared in the density range σ_θ = [28.6 kg m^{-3}, 29.5 kg m^{-3}], when taking into account the penetrative solar radiation in the diagnosis: the transformation rate ($F(\rho)$) of the densest waters increased from 3 Sv with the classical method to 4 Sv with the revised method and covered a wider range (see section 4.1).

[38] As shown in section 4.1, in summer, the transformation rate computed with and without the penetrative solar radiation method are strongly different, especially in the high density range where a water mass formation can occur instead of a destruction with the classical method (Figure 8b). In the light density range, the volume budget is overestimated with the classical method, as in spring. At densities greater than σ_θ = 27 kg m^{-3}, the major effect of the penetrative solar radiation was to transform dense water into lighter water. Indeed, the transformation induced by heat and freshwater flux estimated by the revised method accounts now for the most important part of the destruction of waters of density in the range $\sigma_\theta \geq$ 28 kg m^{-3} with a rate of about 0.5 Sv while the role of the diapycnal fluxes is strongly decreased in this range.

4.3. Water Mass Budgets in the Surface Layers and in the Ocean Interior

[39] The next step was to distinguish between water mass transformation in the surface layers and in the ocean interior. In this way we were able to provide a more accurate estimate of the effective water mass formation, i.e., the water-volume flux into the ocean interior. To this end, we distinguish two control volumes: the first one is defined as the volume of water in the surface layers and the second as the water volume below. Since the only changes attributable to the penetrative solar radiation occur in spring and summer, we focused on these two seasonal budgets. In

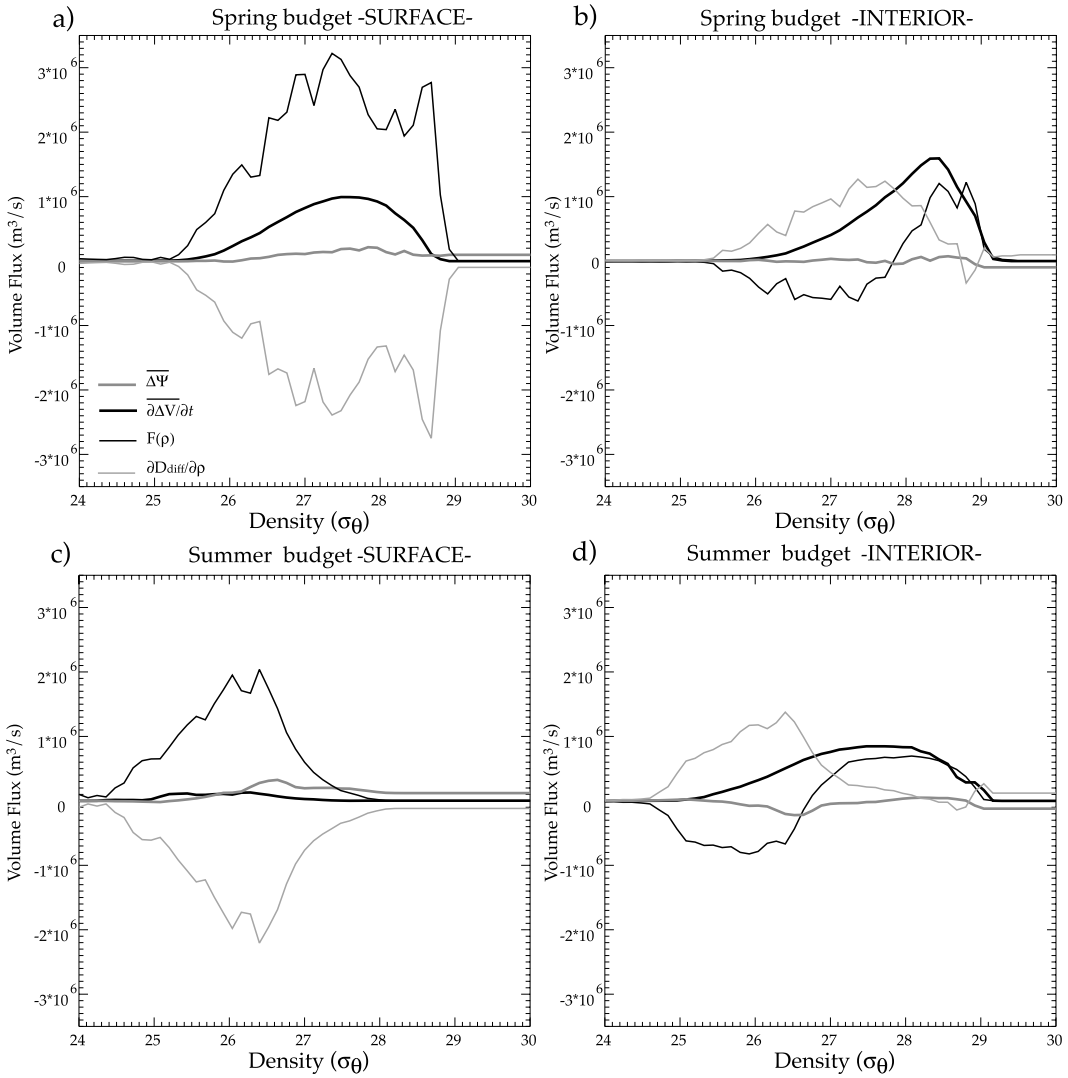

Figure 9. Seasonal water volume budgets versus potential density: (a) in spring for the surface layers (the maximum depth of this layer is equal to 17 m), (b) in spring for the ocean interior, (c) in summer for the surface layers (the maximum depth is equal to 9 m), and (d) in summer for the ocean interior; color-coded lines as in Figure 8. Positive values of the slope are related to the formation of water masses, negative values, to the destruction of water masses.

spring the surface layers are defined by the first 17 m of the ocean surface, corresponding to the first 3 vertical levels of MED8. In summer, these surface layers are set at 9 m, corresponding to the first 2 vertical levels. These surface layers roughly correspond to the mixed layer. Seasonal budgets for spring and summer in the surface layers and in the ocean interior are given in Figure 9. The budgets are averaged over the whole Mediterranean basin, as in the previous section, and are computed using the revised method only.

[40] The strongest volume variations occur in spring, with destruction of the densest water and creation of the lightest water. The transition between newly formed and destroyed water masses differs slightly between the surface layers and the ocean interior, with a potential density of 27.4 kg m^{-3} at the surface and a potential density of 28.4 kg m^{-3} in the interior (Figures 9a and 9b). The net volume flux reaches 1.6 Sv in the interior (Figure 9b) and is about 1 Sv in the surface layers (Figure 9a). The penetrative solar radiation plays a significant role in this evolution since, at depth, the volume transformation rate is induced only by this term. This factor is responsible for most of the transformation of the densest water, $\sigma_\theta > 28.7$ kg m^{-3}, corresponding to about 1 Sv (Figure 9b) into lighter water. It also plays an important role in the creation of water of intermediate density (27.3–28.4 kg m^{-3}) corresponding to a value of nearly 2 Sv in the interior (Figure 9b). This strong transformation rate is, however, significantly counterbalanced by mixing, with the destruction of about 1 Sv of these waters, leading to a net formation of about 1 Sv in this density range. In contrast, mixing contributes mostly to the creation of the lowest-density water, while the penetrative solar radiation contributes to its destruction.

[41] In summer, most of the volume variations occur in the ocean interior. At the surface, the transformation rate and diapycnal fluxes terms are almost balanced. These two

terms play alternating roles, depending on the density range: water in the smaller density range were created by atmospheric fluxes and destroyed by mixing; and conversely, waters in the higher density range were created by mixing and destroyed by atmospheric fluxes. In the ocean interior, a similar pattern to that obtained in spring was observed. Thus the analysis reveals the important role of the penetrative solar radiation below the surface layers under the stratified conditions of spring and summer. Basically, this factor contributes to the destruction of the highest- and lowest-density water and to the creation of the intermediate-density water.

5. Conclusions

[42] In this work, we focused on the estimate of the impact of the penetrative solar radiation on the determination of water mass transformation in the Mediterranean Sea. Water mass transformation is a key process that drives the Mediterranean thermohaline circulation and thus requires accurate estimation**.** We used the simulation results of a 1/8° resolution oceanic model that takes into account the penetration of the solar radiation with respect to depth. In order to respect the adequacy between the prognostic model MED8 and the diagnostic method, we applied a revised diagnosis, based on the Walin's method for the estimate of water mass transformation, that takes into account this vertical penetration of the solar radiation. This model was forced with ECMWF atmospheric fields, which allows a good representation of the oceanic circulation and of air-sea exchanges. We first compared the annual water mass transformation rate computed with the revised method with that obtained with the classical method. Major differences in estimates are observed, depending on the method applied, with a strong decrease in water mass transformation of about 40–50% in agreement with the global ocean analysis presented by *Iudicone et al.* [2008].

[43] This decrease results from the lower seasonal variation when the penetrative solar radiation is considered. This can be explained by the fact that the solar radiation is then calculated over a wider density range, leading to weaker net values over a given density range. As well mixing that counterbalances production was previously overestimated in the annual budget. The greatest impact of the penetrative solar radiation occurs in spring and summer when the stratification of the water column is strong. Newly formed dense water is destroyed, at a rate of about 50% of the rate in winter.

[44] We computed water mass volume budgets during these two seasons. The two terms that are responsible for the volume variation are the transformation rate due to atmospheric fluxes (i.e., $F(\rho)$) and the interior mixing (i.e., diapycnal fluxes). The most striking change observed was for the densest water masses (>27 kg/m^3) in summer. The penetrative solar radiation is therefore responsible for the destruction of these water masses, whereas, with the classical method, only mixing could play this role. In spring, mixing was previously underestimated for these densest waters. Regarding the light density range, mixing and transformation rate were previously overestimated both in spring and summer. We also show that about 1/3 of the water mass transformation takes place below the surface layers.

[45] In this study, we give evidence of the crucial effect of taking into account the penetrative solar flux on water mass transformation diagnosis in the Mediterranean Sea. The next step for improving this effect would rely on a better parameterization of the penetration of the solar radiation in the prognostic model and in the diagnosis, possibly by including the variation in the absorption of the incoming solar radiation by the phytoplanktonic organisms in the water column which modulates the transparency of the seawater in space and time. The importance of this variation in the Mediterranean was shown by *Bosc et al.* [2004] from satellite ocean color-sensor data. We are also aware that our conclusions are sensitive to the vertical discretization of the model. This point is very delicate to investigate and should need to run again the prognostic model with a refine vertical grid which is beyond the scope of the present paper.

[46] **Acknowledgments.** We would like to thank K. Béranger, L. Li and G. Madec for fruitful discussions. We acknowledge financial support from the French national program GICC (Gestion et Impact du Changement Climatique) and the French Mercator project (www.mercator-ocean.fr). ECMWF analyses were kindly made available by the European Centre for Medium-range Weather Forecasts. Numerical simulations were performed on the NEC SX-5 of the Institut du Développement et des Ressources en Informatique Scientifique (IDRIS) of the Centre National de la Recherche Scientifique (CNRS). We thank Ray C. Griffiths for editing this manuscript.

References

Alhammoud, B., K. Béranger, L. Mortier, M. Crépon, and I. Dekeyser (2005), Surface circulation of the Levantine Basin: Comparison of models results with observations, *Prog. Oceanogr.*, *66*, 299–320.

Artegiani, A., D. Bregant, E. Paschini, N. Pinardi, F. Raicich, and A. Russo (1997), The Adriatic Sea general circulation. Part I: Air-sea interactions and water mass structure, *J. Phys. Oceanogr.*, *27*, 1492–1514.

Astraldi, M., G. P. Gasparini, A. Vetrano, and S. Vignudelli (2002), Hydrographic characteristics and interannual variability of water masses in the central Mediterranean: A sensitivity test for long-term changes in the Mediterranean Sea, *Deep Sea Res., Part I*, *49*, 661–680.

Barnier, B., L. Siefrid, and P. Marchesiello (1995), Thermal forcing for a global ocean circulation model using a three-year climatology of ECMWF analyses, *J. Mar. Syst.*, *6*, 363–380.

Béranger, K., L. Mortier, L. Gervasio, G. P. Gasparini, M. Astraldi, and M. Crépon (2004), The surface circulation dynamics of the Sicily Strait: A comprehensive study from the observations to the models, the role of the topography, *Deep Sea Res., Part II*, *51*, 411–440.

Béthoux, J. P. (1979), Budgets of the Mediterranean Sea. Their dependence on the local climate and on the characteristics of the Atlantic waters, *Oceanol. Acta*, *2*, 157–163.

Blanke, B., and P. Delecluse (1993), Variability of the tropical Atlantic Ocean simulated by a general circulation model with two different mixed layer physics, *J. Phys. Oceanogr.*, *23*, 1363–1388.

Bosc, E., A. Bricaud, and D. Antoine (2004), Seasonal and interannual variability in algal biomass and primary production in the Mediterranean Sea, as derived from 4 years of SeaWiFS observations, *Global Biogeochem. Cycles*, *18*, GB1005, doi:10.1029/2003GB002034.

Drillet, Y., K. Béranger, M. Brémond, F. Gaillard, C. Le Provost, L. Siefridt, and S. Theetten (2000), Expérimentation PAM, in *Tech. Rep. MERCATOR Proj.*, CERFACS, Toulouse, France.

Frouin, R., and S. F. Iacobellis (2002), Influence of phytoplankton on the global radiation budget, *J. Geophys. Res.*, *107*(D19), 4377, doi:10.1029/2001JD000562.

Fuda, J. L., C. Millot, I. Taupier-Letage, U. Send, and J. M. Bocognano (2000), XBT monitoring of a meridian section across the western Mediterranean Sea, *Deep Sea Res., Part I*, *47*, 2191–2218.

Garrett, C., R. Outerbridge, and K. Thompson (1993), Interannual variability in Mediterranean heat and buoyancy fluxes, *J. Clim.*, *6*, 900–910.

Gertman, I. F., I. M. Ovchinnikov, and Yu. I. Popov (1994), Deep convection in the eastern basin of the Mediterranean Sea, *Oceanology*, *34*, 19–24.

Horton, C., J. Kerling, G. Athey, J. Schmitz, and M. Clifford (1994), Airborne expendable bathythermograph surveys of the eastern Mediterranean, *J. Geophys. Res.*, *99*, 9891–9905.

Iudicone, D., G. Madec, and T. J. McDougall (2008), Diagnosing water transformations and the key role of light penetration, *J. Phys. Oceanogr.*, in press.

Jerlov, N. G. (1968), *Optical Oceanography*, 194 pp., Elsevier, New York.

Lacombe, H., and P. Tchernia (1972), Caractères hydrologiques et circulation des eaux en Méditerranée, in *Mediterranean Sea*, edited by D. J. Stanley, pp. 25–36, Hutchinson and Ross, Strasburg.

Large, W. G., and A. J. G. Nurser (2001), Ocean surface water mass transformation, in *Ocean Circulation and Climate*, pp. 317–336, Academic Press, New York.

Lascaratos, A., W. Roether, K. Nittis, and B. Klein (1999), Recent changes in deep water formation and spreading in the eastern Mediterranean Sea: A review, *Prog. Oceanogr.*, *44*, 5–36.

Lévy, M., A. Estublier, and G. Madec (2001), Choice of an advection scheme for biogeochemical models, *Geophys. Res. Lett.*, *28*, 3725–3728.

Lewis, M. R., M.-E. Carr, G. C. Feldman, W. Esaias, and C. McClain (1990), Influence of the penetrating solar radiation on the heat budget of the equatorial Pacific Ocean, *Nature*, *347*, 543–545.

MacDonald, A., J. Candela, and H. L. Bryden (1994), An estimate of the net heat transport through the Strait of Gibraltar, in *Coastal Estuarine Stud.*, vol. 46, edited by P. E. La Violette, pp. 13–32, AGU, Washington, D. C.

Madec, G., F. Lott, P. Delecluse, and M. Crépon (1996), Large-scale preconditioning of deep-water formation in the northwestern Mediterranean Sea, *J. Phys. Oceanogr.*, *26*, 1393–1408.

Madec, G., P. Delecluse, M. Imbard, and C. Lévy (1998), OPA8.1, in *Ocean General Circulation Model, Reference Manual*, 97 pp., Note du Pôle de modélisation de l'IPSL, Paris.

Marshall, J. C., A. J. G. Nurser, and R. G. Williams (1993), Inferring the subduction rate and period over the North Atlantic, *J. Phys. Oceanogr.*, *23*, 1315–1329.

MEDAR/MEDATLAS Group (2002), *MEDAR/MEDATLAS 2002 Database. Cruise inventory, observed and analysed data of temperature and bio-chemical parameters* [CD-ROM], IFREMER Ed., Brest, France.

MEDOC Group (1970), Observation of formation of deep water in the Mediterranean Sea, *Nature*, *227*, 1037–1040.

Mertens, C., and F. Schott (1998), Interannual variability of deep-water formation in the northwestern Mediterranean, *J. Phys. Oceanogr.*, *28*, 1410–1424.

Millot, C. (1999), Circulation in the western Mediterranean Sea, *J. Mar. Syst.*, *20*, 423–442.

Morel, A., and D. Antoine (1994), Heating rate within the upper ocean in relation to its bio-optical state, *J. Phys. Oceanogr.*, *24*, 1652–1665.

Murtugudde, R., J. Beauchamp, C. R. McClain, M. Lewis, and A. J. Busalacchi (2002), Effects of penetrative radiation on the upper tropical ocean circulation, *J. Clim.*, *15*, 470–486.

Nurser, A. J. G., R. Marsh, and R. G. Williams (1999), Diagnosing water mass formation from air-sea fluxes and surface mixing, *J. Phys. Oceanogr.*, *29*, 1468–1487.

Pacanowski, R. C., and A. Gnanadesikan (1998), Transient response in a Z-level ocean model that resolve topography with partial cells, *Mon. Weather Rev.*, *126*, 3248–3270.

Poulain, P.-M. (2001), Adriatic Sea surface circulation as derived from drifter data between 1990 and 1999, *J. Mar. Syst.*, *29*, 3–32.

Reynolds, R. W. (1988), A real-time global sea surface temperature analysis, *J. Clim.*, *1*, 75–86.

Robinson, A. R., J. Sellschopp, A. Warn-Varnas, W. G. Leslie, C. J. Lozano, P. J. Haley Jr., L. A. Anderson, and P. F. J. Lermusiaux (1999), The atlantic ionian stream, *J. Mar. Syst.*, *20*, 129–156.

Roether, W., and R. Schlitzer (1991), Eastern Mediterranean deep water renewal on the basis of chlorofluoromethanes and tritium, *Dyn. Atmos. Oceans*, *15*, 333–354.

Roether, W., B. Klein, V. Beitzel, and B. B. Manca (1998), Property distributions and transient tracer ages in levantine intermediate water in the eastern Mediterranean, *J. Mar. Syst.*, *18*, 71–87.

Schott, F. A., and K. D. Leaman (1991), Hydrographic structure of the convection regime in the Gulf of Lions: Winter 1987, *J. Phys. Oceanogr.*, *21*, 575–598.

Siefridt, L., Y. Drillet, R. Bourdalle-Badie, K. Béranger, C. Talatier, and E. Greiner (2002), Implementation of the high-resolution MERCATOR model for the North Atlantic and Mediterranean regions, in the *MERCATOR Quarterly Newsletter no. 5*, pp. 1–12, Toulouse.

Theocharis, A., B. Klein, K. Nittis, and W. Roether (2002), Evolution of the eastern Mediterranean transient (1997–1999), *J. Mar. Syst.*, *33–34*, 91–116.

Tziperman, E. (1986), On the role of interior mixing and air-sea fluxes in determining the stratification and circulation of the oceans, *J. Phys. Oceanogr.*, *16*, 680–693.

Tziperman, E., and K. Speer (1994), A study of water mass transformation in the Mediterranean Sea: Analysis of climatological data and a simple three-box model, *Dyn. Atmos. Oceans*, *21*, 53–82.

Vargas-Yañez, M., F. Plaza, J. Garcia-Lafuente, T. Sarhan, J. M. Vargas, and P. Velez-Belchi (2000), About the seasonal variability of the Alboran Sea circulation, *J. Mar. Syst.*, *35*, 229–248.

Vilibic, I., and M. Orlic (2002), Adriatic water masses, their rates of formation and transport through the Otranto Strait, *Deep Sea Res., Part I*, *49*, 1321–1340.

Walin, G. (1982), On the relation between sea-surface heat flow and the thermal circulation in the ocean, *Tellus, Ser. A and Ser. B*, *34*, 187–195.

Wust, G. (1961), On the vertical circulation of the Mediterranean Sea, *J. Geophys. Res.*, *66*, 3261–3271.

P. Bouruet-Aubertot and M. Crépon, Laboratoire d'Océanographie et de Climatologie - Expérimentation et Applications Numériques, LOCEAN/IPSL (previously LODYC), T46 5E Case 100, 4 place Jussieu, 75252 Paris Cedex 05, France.

A. Bozec, COAPS, Florida State University, 222 Room Johnson Building, 2035 E. Paul Dirac Drive, Tallahassee, FL 32310, USA. (abozec@coaps.fsu.edu)

D. Iudicone, Laboratory of Biological Oceanography, Stazione Zoologica, SZN, Villa Comunale, 80121 Naples, Italy.